Sensors and Materials, Vol. 34, No. 2 (2022) 585–593
MYU Tokyo

S & M 2830

Effect of Cu Doping on Photoluminescence and Scintillation Properties of $(C_6H_5C_2H_4NH_3)_2PbBr_4$

Daichi Onoda,[1*] Masaki Akatsuka,[1] Naoki Kawano,[2] Takumi Kato,[1]
Daisuke Nakauchi,[1] Noriaki Kawaguchi,[1] and Takayuki Yanagida[1]

[1]Division of Materials Science, Nara Institute of Science and Technology (NAIST),
8916-5 Takayama-Cho, Ikoma, Nara 630-0192, Japan
[2]Graduate School of Engineering Science, Akita University,
1-1 Tegatagakuen-machi, Akita City, Akita 010-8502, Japan

(Received October 5, 2021; accepted October 21, 2021)

Keywords: photoluminescence, scintillation, quantum-well structure, organic lead halide perovskite, Cu

The photoluminescence (PL) and scintillation properties of $(C_6H_5C_2H_4NH_3)_2Pb_{1-x}Cu_xBr_4$ (x = 0.05, 0.1, 0.25, and 0.5) single crystals prepared by the poor-solvent diffusion method were evaluated. In the PL profiles, free- and bound-exciton luminescence peaks at 410 and 440 nm were observed, respectively. The PL quantum yields (*QYs*) of the x = 0.05, 0.1, 0.25, and 0.5 samples were 20.0, 19.3, 18.4, and 16.7% with 2% errors, respectively. In the scintillation profiles, a bound-exciton luminescence peak was observed at 440 nm. Under γ-ray exposure with ^{137}Cs, a photoabsorption peak was observed in all the samples, and the scintillation light yields of the x = 0.05, 0.1, 0.25, and 0.5 samples were estimated to be ~12000, ~11000, ~10000, and ~9700 ph/MeV with 10% errors, respectively.

1. Introduction

Scintillators instantaneously convert ionizing radiation to low-energy photons; thus, when coupled with a photodetector, they can be used as radiation detectors in a wide range of fields including medical imaging, security, biology, and astrophysics.[1–4] Typical requirements for scintillators are short luminescence lifetime, low afterglow, high light yield (*LY*), large effective atomic number, and high density.[5] Ideally, all these requirements are satisfied; however, such perfect scintillators do not exist at present. Hence, users select an appropriate one in accordance with their purpose, and continuous efforts have been made to develop new scintillators with better properties.[6–11]

Today, rapid-response scintillators are in strong demand since high timing resolution is required for some applications,[12,13] and semiconductor materials can be used as such scintillators.[14,15] In these materials, Wannier-type excitons are generated by the irradiation of radiation, and the luminescence generated by their recombination has an extremely short lifetime, generally of nanosecond order. However, a major problem is that the exciton luminescence in these materials is easily quenched, even at room temperature, owing to the low

*Corresponding author: e-mail: onoda.daichi.ob3@ms.naist.jp
https://doi.org/10.18494/SAM3679

ISSN 0914-4935

exciton binding energy. With this background, 2D organic lead halide perovskites $(R\mathrm{NH_3})_2\mathrm{Pb}X_4$ (*R*: hydrocarbon, *X*: halogen) have attracted a lot of attention.[16,17] These materials have a structure with an inorganic layer consisting of corner-sharing $\mathrm{Pb}X_6^{2-}$ octahedra sandwiched between organic layers, and the bandgap energy of the inorganic layer is much lower than that of the organic layers; thus, the structure can be regarded as a quantum-well structure where the organic and inorganic layers act as barrier and well layers, respectively.[18,19] Excitons confined in such a structure have enhanced binding energy; thus, fast and efficient luminescence can be achieved even at room temperature. Numerous studies of these materials have been carried out for around two decades,[20–22] and it has recently been demonstrated that the scintillation properties of $(R\mathrm{NH_3})_2\mathrm{PbBr_4}$ can be improved by increasing the exciton localization due to the structural distortion of the inorganic layer (changes of Br–Pb–Br and Pb–Br–Pb bond angles).[23,24] Moreover, it has been reported that $(\mathrm{C_6H_5C_2H_4NH_3})_2\mathrm{PbBr_4}$ shows a particularly high scintillation *LY* (~14000 ph/MeV) compared with other $(R\mathrm{NH_3})_2\mathrm{PbBr_4}$ owing to the structural distortion of the inorganic layer.[24,25] From these reports, with the aim of improving the scintillation properties of $(\mathrm{C_6H_5C_2H_4NH_3})_2\mathrm{PbBr_4}$, our group has conducted studies of cation doping in $(\mathrm{C_6H_5C_2H_4NH_3})_2\mathrm{PbBr_4}$ to induce further distortion of the inorganic layer, and some attempts have successfully enhanced *LY*.[26–31]

In the present study, we chose $\mathrm{Cu^{2+}}$ as a cation for doping into the inorganic layer of $(\mathrm{C_6H_5C_2H_4NH_3})_2\mathrm{PbBr_4}$. Six-coordinated $\mathrm{Cu^{2+}}$ has an ionic radius of 0.073 nm, which is much smaller than that of $\mathrm{Pb^{2+}}$ (0.119 nm).[32] Thus, we expected that Cu doping would be effective for inducing further distortion of the inorganic layer. We prepared $(\mathrm{C_6H_5C_2H_4NH_3})_2\mathrm{Pb_{1-}}_x\mathrm{Cu}_x\mathrm{Br_4}$ single crystals and evaluated their photoluminescence (PL) and scintillation properties.

2. Materials and Methods

2.1 Sample preparation

$(\mathrm{C_6H_5C_2H_4NH_3})_2\mathrm{Pb_{1-}}_x\mathrm{Cu}_x\mathrm{Br_4}$ single crystals with different Cu amounts (x = 0.05, 0.1, 0.25, and 0.5) were prepared by a previously reported procedure.[33] $\mathrm{C_6H_5C_2H_4NH_2}$ (99%, Alfa Aesar), HBr acid (47.0–49.0 wt%, Wako Pure Chemical Industries), $\mathrm{PbBr_2}$ (99.999%, Pro Chem, Inc.), and $\mathrm{CuBr_2}$ (99.9%, High Purity Chemicals) were used as starting materials, and *N,N*-dimethylformamide (>99.5%, Wako Pure Chemical Industries) and nitromethane (>96.0%, Wako Pure Chemical Industries) were used as good and poor solvents, respectively.

2.2 Property evaluation

To investigate the structure, X-ray diffraction (XRD) analyses were carried out with an X-ray diffractometer (Miniflex600, Rigaku) in a 2θ range of 3–50 degrees. Diffuse transmission spectra were recorded by a spectrophotometer (SolidSpec-3700, SHIMADZU) in the range of 250–850 nm.

PL quantum yields (*QY*s) and spectra were recorded by a Quantaurus-*QY* (C11347, Hamamatsu), where the excitation and emission ranges were 250–500 and 300–600 nm,

respectively. PL decay profiles were recorded by a Quantaurus-τ (C11367, Hamamatsu), where the signals were collected at 440 nm upon excitation at 365 nm.

Scintillation spectra during X-ray exposure were recorded by our original setup, where the tube voltage and tube current were set at 40 kV and 1.2 mA, respectively.[34] Scintillation decay profiles and afterglow profiles under X-ray exposure were recorded by our original setup, where the tube voltage was set at 30 kV.[35] Pulse height spectra under 662 keV γ-rays from ^{137}Cs exposure were recorded by our original setup.[36] In some of the characterizations below, an x = 0 sample (thickness: ~1 mm) prepared in a previous work[25] was used for comparison.

3. Results and Discussion

3.1 Samples

$(C_6H_5C_2H_4NH_3)_2Pb_{1-x}Cu_xBr_4$ samples were successfully obtained as shown in Fig. 1. The samples were transparent and slightly yellow, and the thicknesses of the x = 0.05, 0.1, 0.25, and 0.5 samples were ~0.7, ~0.6, ~0.6, and ~0.5 mm, respectively.

Some of the obtained samples were crushed into powder, and their XRD patterns were measured as shown in Fig. 2(a). All the samples showed diffraction patterns with peaks in a regular interval, where each peak corresponded to the (0 0 2l) plane (l = 1–7). From the results, we confirmed that a quantum-well structure was formed in the samples.[25] To enable a detailed discussion, enlarged views of the (0 0 10) peaks are shown in Fig. 2(b) with those of the x = 0 sample. The ionic radii of six-coordinated Cu^{2+} and Pb^{2+} are 0.073 and 0.119 nm, respectively; thus, the lattice constants should monotonically decrease with increasing Cu content. However, the present results did not show such a trend. This is probably because complicated structural changes occurred not only in the inorganic layer but also in the organic layer.[37]

Diffuse transmission spectra of the $(C_6H_5C_2H_4NH_3)_2Pb_{1-x}Cu_xBr_4$ samples are shown in Fig. 3. A spectrum of the x = 0 sample is also shown. All the Cu-doped samples showed transmittance of around 80% in the visible range and absorption around 250–430 nm. By comparison with the absorption spectrum of $(C_6H_5C_2H_4NH_3)_2PbBr_4$, the absorption was

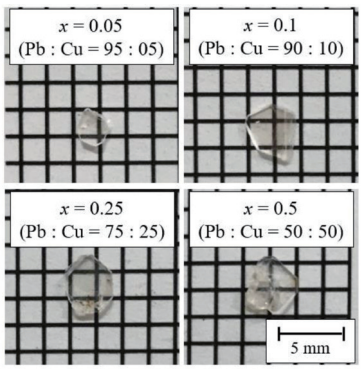

Fig. 1. (Color online) Appearances of the $(C_6H_5C_2H_4NH_3)_2Pb_{1-x}Cu_xBr_4$ samples.

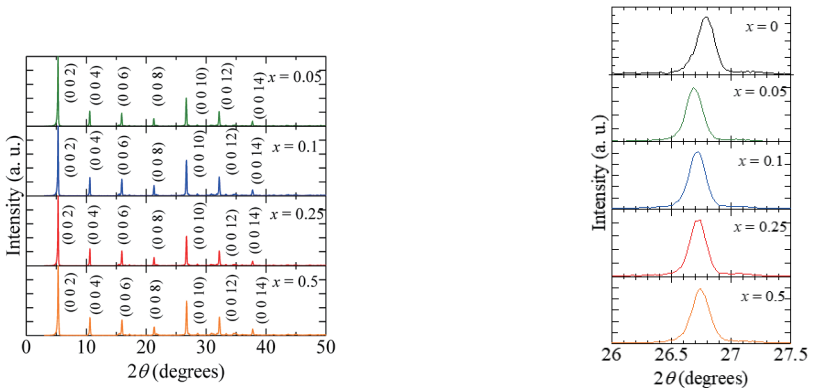

Fig. 2. (Color online) XRD patterns of the $(C_6H_5C_2H_4NH_3)_2Pb_{1-x}Cu_xBr_4$ samples in ranges of (a) 3–50 and (b) 26–27.5 degrees.

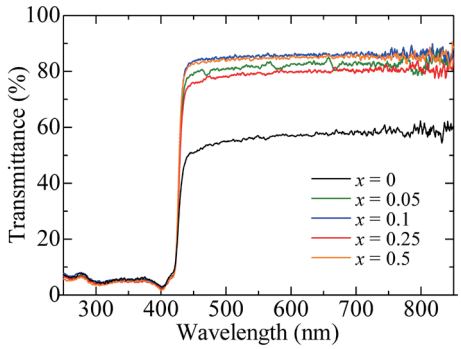

Fig. 3. (Color online) Diffuse transmission spectra of the $(C_6H_5C_2H_4NH_3)_2Pb_{1-x}Cu_xBr_4$ samples.

ascribed to electronic transitions from Pb(6s)/Br(4p) mixed states to mainly Pb(6p) states in the inorganic layer.[38]

3.2 PL properties

Figure 4 shows a PL spectrum of the $(C_6H_5C_2H_4NH_3)_2Pb_{0.95}Cu_{0.05}Br_4$ (x = 0.05) sample. Here, a selected spectrum is shown as a representative because no difference in the spectral shape was confirmed among the samples. When the sample was excited at 270–430 nm, two luminescence peaks appeared at 410 and 440 nm. Since the spectral shape was in agreement with that of undoped and other cation-doped $(C_6H_5C_2H_4NH_3)_2PbBr_4$,[29,33,39,40] the former and latter peaks were derived from free excitons and bound excitons at shallow trapping states, respectively. The PL *QY* values of the x = 0.05, 0.1, 0.25, and 0.5 samples were 20.0, 19.3, 18.4, and 16.7% with 2% errors, respectively, which were lower than that of $(C_6H_5C_2H_4NH_3)_2PbBr_4$ (~22%) reported previously.[25] In a previous study, it was demonstrated that radiative decay rates increased owing to the decrease in Br–Pb–Br and Pb–Br–Pb bond angles.[23] From the XRD peaks in Fig. 2(b), we can confirm that a structural change occurred in the samples. For these reasons, it is considered that Cu doping will increase the Br–Pb–Br or Pb–Br–Pb bond

angle. It is also considered that Cu doping will generate lattice defects and increase the number of nonradiative transitions.

Figure 5 shows PL decay profiles of the $(C_6H_5C_2H_4NH_3)_2Pb_{1-x}Cu_xBr_4$ samples. Under excitation at 365 nm, decay profiles with three different lifetimes were obtained for all the samples. The lifetimes of the first components (τ_1) were typical values of free-exciton luminescence.[25,27] The second (τ_2) and third (τ_3) components had relatively long lifetimes, which were derived from bound excitons at shallow trapping states.[27] The ratios of the first (τ_1): second (τ_2): third (τ_3) components in the x = 0.05, 0.1, 0.25, and 0.5 samples were 80.1: 19.3: 0.6, 80.9: 18.6: 0.6, 78.5: 20.9: 0.6, and 78.3: 21.1: 0.6%, respectively. The obtained free-exciton luminescence had both an extremely short lifetime and a narrow linewidth. Generally, free excitons confined in a quantum well have low flexibility; thus, the kinetic energy becomes low, resulting in a sharp luminescence peak. In addition, such excitons have high binding energy and large oscillator strength owing to the quantum-confinement effect; therefore, fast decay can also be achieved.

3.3 Scintillation properties

Figure 6 shows scintillation spectra of the $(C_6H_5C_2H_4NH_3)_2Pb_{1-x}Cu_xBr_4$ samples under X-ray exposure. In all the samples, a luminescence peak was observed at 440 nm. By comparison of the PL results, we concluded that the peak was derived from bound excitons at shallow trapping states. Here, the free-exciton luminescence peak that appeared at 410 nm in the PL spectra was not observed. We concluded that this was due to self-absorption because similar phenomena were reported previously.[30,33] The PL spectra were measured in a reflection-type geometric arrangement, where the observed photons were emitted from the same surface of the sample as that on which the excitation photons were incident. On the other hand, the scintillation spectra were measured by a transmission-type geometric arrangement, where the scintillation photons transmitted through the sample were detected. The difference in the measurement geometries explained why self-absorption occurred only in the scintillation.

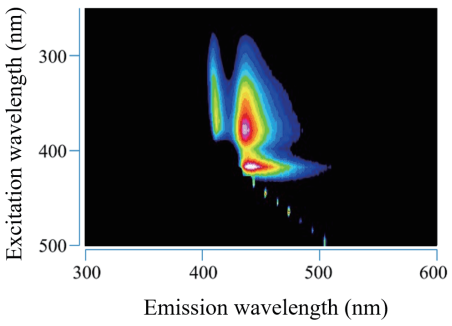

Fig. 4. (Color online) PL spectrum of the $(C_6H_5C_2H_4NH_3)_2Pb_{0.95}Cu_{0.05}Br_4$ sample, where the vertical and horizontal axes represent excitation and emission wavelengths, respectively.

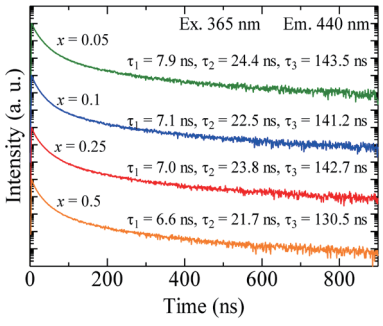

Fig. 5. (Color online) PL decay profiles of the $(C_6H_5C_2H_4NH_3)_2Pb_{1-x}Cu_xBr_4$ samples. The signals were collected at 440 nm upon excitation at 365 nm.

Figure 7 shows scintillation decay profiles of the $(C_6H_5C_2H_4NH_3)_2Pb_{1-x}Cu_xBr_4$ samples under X-ray exposure. As with the PL profiles, the obtained decay profiles had three different lifetimes. The first component (τ_1) was assigned to free excitons, and the second (τ_2) and third (τ_3) ones were attributed to bound excitons at shallow trapping states.[26,29] Longer lifetimes were obtained from the scintillation decay profiles than those from the PL results. Scintillation has an energy-transportation process in addition to a luminescence process (PL), and this additional process is considered to contribute to the slower scintillation decay. The lifetimes of the first components were comparable to that of $(C_6H_5C_2H_4NH_3)_2PbBr_4$ (~11 ns)[25] and were much shorter than those of most practical scintillators including Lu_2SiO_5:Ce (~40 ns) and $Bi_4Ge_3O_{12}$ (~300 ns).[2] The ratios of the first (τ_1): second (τ_2): third (τ_3) components in the x = 0.05, 0.1, 0.25, and 0.5 samples were 76.2: 22.4: 1.4, 81.5: 17.1: 1.4, 81.4: 17.1: 1.5, and 78.8: 19.8: 1.4% respectively.

Figure 8 shows afterglow profiles of the $(C_6H_5C_2H_4NH_3)_2Pb_{1-x}Cu_xBr_4$ samples under X-ray irradiation. To evaluate the afterglow properties, the afterglow level (AL) was defined as AL (ppm) = $10^6 \times (I_{20} - I_{BG})/(I_{max} - I_{BG})$, where I_{20}, I_{max}, and I_{BG} denote the signal intensity at 20 ms after X-ray cutoff, the average value during X-ray irradiation, and the value before X-ray irradiation, respectively. The AL values of the x = 0.05, 0.1, 0.25, and 0.5 samples were estimated using the formula to be ~32, ~44, ~29, and ~31 ppm, respectively. In a previous study, AL of $(C_6H_5C_2H_4NH_3)_2PbBr_4$ was reported to be ~5 ppm,[25] and the present results were inferior. In afterglow, carriers trapped at shallow states are re-excited around room temperature. Therefore, the present results suggest that the number of trapping states was increased by Cu doping.

Figure 9 shows pulse height spectra of the $(C_6H_5C_2H_4NH_3)_2Pb_{1-x}Cu_xBr_4$ samples including that of an x = 0 sample prepared in a previous study.[25] Under 662 keV γ-rays from ^{137}Cs exposure, all the samples showed a photoabsorption peak. Compared with the LY value of ~14000 ph/MeV for the x = 0 sample, we obtained values of ~12000, ~11000, ~10000, and ~9700 ph/MeV with 10% errors for the x = 0.05, 0.1, 0.25, and 0.5 samples, respectively, by comparing the photoabsorption peak channels. The lower LY values than that of the x = 0 sample were consistent with the PL QY values. LY can be theoretically expressed as $LY = 10^6 \times S \times QY/(\beta \times E_g)$,

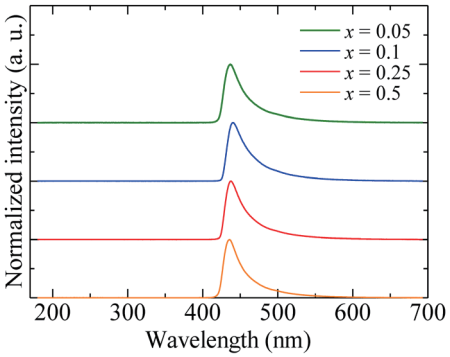

Fig. 6. (Color online) Scintillation spectra of the $(C_6H_5C_2H_4NH_3)_2Pb_{1-x}Cu_xBr_4$ samples under X-ray exposure.

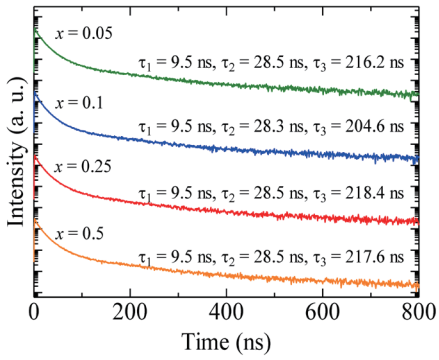

Fig. 7. (Color online) Scintillation decay profiles of the $(C_6H_5C_2H_4NH_3)_2Pb_{1-x}Cu_xBr_4$ samples under X-ray exposure.

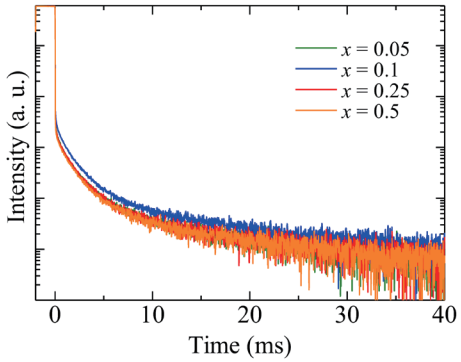

Fig. 8. (Color online) Afterglow profiles of the $(C_6H_5C_2H_4NH_3)_2Pb_{1-x}Cu_xBr_4$ samples under X-ray exposure.

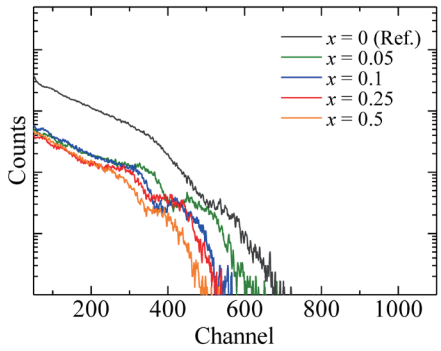

Fig. 9. (Color online) Pulse height spectra of the $(C_6H_5C_2H_4NH_3)_2Pb_{1-x}Cu_xBr_4$ samples under 662 keV γ-rays from ^{137}Cs exposure.

where S, QY, β, and E_g are the energy-transportation efficiency from a host to luminescent states, the PL QY, a constant parameter, and the bandgap energy, respectively.[41] On the basis of the formula, it is considered that the low PL QY values are one of the reasons for the low LY values.

4. Conclusions

$(C_6H_5C_2H_4NH_3)_2Pbl_{-x}Cu_xBr_4$ (x = 0.05, 0.1, 0.25, and 0.5) single crystals were successfully obtained by the poor-solvent diffusion method, and their PL and scintillation properties were evaluated. In the PL profiles, two luminescence peaks related to free and bound excitons were observed. The PL QY values of the x = 0.05, 0.1, 0.25, and 0.5 samples were 20.0, 19.3, 18.4, and 16.7% with 2% errors, respectively, which were lower than that of $(C_6H_5C_2H_4NH_3)_2PbBr_4$ (~22%) reported previously. In the scintillation profiles, a bound-exciton luminescence peak was observed under X-ray exposure. Under γ-ray exposure, a photoabsorption peak was observed for all the samples, and the LY values of the x = 0.05, 0.1, 0.25, and 0.5 samples were estimated to be ~12000, ~11000, ~10000, and ~9700 ph/MeV with 10% errors, respectively, which were lower than that of $(C_6H_5C_2H_4NH_3)_2PbBr_4$ (~14000 ph/MeV). As a result, Cu doping deteriorated the PL and scintillation properties of $(C_6H_5C_2H_4NH_3)_2PbBr_4$.

Acknowledgments

This work was supported by Grants-in-Aid for Scientific Research, Scientific Research B (19H03533, 21H03733, and 21H03736), Early-Career Scientists (20K20104 and 20K15026), and JSPS Fellows (19J22402) from JSPS. The Cooperative Research Project of the Research Center for Biomedical Engineering, Nippon Sheet Glass Foundation, SEI Group CSR Foundation, Yashima Environment Technology Foundation, Okura Kazuchika Foundation, and Hitachi Metals-Materials Science Foundation are also acknowledged.

References

1 T. Yanagida: Proc. Japan Acad. Ser. B **94** (2018) 75. https://doi.org/10.2183/pjab.94.007
2 C. W. E. van Eijk: Nucl. Instrum. Methods Phys. Res., Sect. A **460** (2001) 1. https://doi.org/10.1016/S0168-9002(00)01088-3
3 M. Kitano, S. Yamamoto, T. Yabe, T. Akagi, T. Toshito, M. Yamaguchi, and N. Kawachi: J. Instrum. **16** (2021) P08064. https://doi.org/10.1088/1748-0221/16/08/P08064
4 T. Matsubara, T. Yanagida, N. Kawaguchi, T. Nakano, J. Yoshimoto, M. Sezaki, H. Takizawa, S. P. Tsunoda, S. Horigane, S. Ueda, S. Takemoto-Kimura, H. Kandori, A. Yamanaka, and T. Yamashita: Nat. Commun. **12** (2021) 4478. https://doi.org/10.1038/s41467-021-24717-1
5 S. E. Derenzo, M. J. Weber, E. Bourret-Courchesne, and M. K. Klintenberg: Nucl. Instrum. Methods Phys. Res., Sect. A **505** (2003) 111. https://doi.org/10.1016/S0168-9002(03)01031-3
6 M. Akatsuka, H. Kimura, D. Onoda, D. Shiratori, D. Nakauchi, T. Kato, N. Kawaguchi, and T. Yanagida: Sens. Mater. **33** (2021) 2243. https://doi.org/10.18494/sam.2021.3319
7 H. Fukushima, M. Akatsuka, H. Kimura, D. Onoda, D. Shiratori, D. Nakauchi, T. Kato, N. Kawaguchi, and T. Yanagida: Sens. Mater. **33** (2021) 2235. https://doi.org/10.18494/sam.2021.3324
8 T. Yanagida, Y. Fujimoto, M. Arai, M. Koshimizu, T. Kato, D. Nakauchi, and N. Kawaguchi: Sens. Mater. **32** (2020) 1351. https://doi.org/10.18494/SAM.2020.2711
9 N. Kawaguchi, H. Masai, M. Akatsuka, D. Nakauchi, T. Kato, and T. Yanagida: Sens. Mater. **33** (2021) 2215. https://doi.org/10.18494/sam.2021.3410
10 D. Nakauchi, T. Kato, N. Kawaguchi, and T. Yanagida: Sens. Mater. **32** (2020) 1389. https://doi.org/10.18494/SAM.2020.2751
11 K. Okazaki, D. Onoda, H. Fukushima, D. Nakauchi, T. Kato, N. Kawaguchi, and T. Yanagida: J. Mater. Sci. Mater. Electron. **32** (2021) 21677. https://doi.org/10.1007/s10854-021-06686-9
12 K. Takahashi, M. Arai, M. Koshimizu, Y. Fujimoto, T. Yanagida, and K. Asai: Jpn. J. Appl. Phys. **59** (2020) 072002. https://doi.org/10.35848/1347-4065/ab9655
13 S. Surti and J. S. Karp: Phys. Medica. **80** (2020) 251. https://doi.org/10.1016/j.ejmp.2020.10.031
14 T. Yanagida, T. Kato, D. Nakauchi, G. Okada, and N. Kawaguchi: Appl. Phys. Express. **14** (2021). https://doi.org/10.35848/1882-0786/ac13d8
15 T. Yanagida, Y. Fujimoto, K. Yamanoi, M. Kano, A. Wakamiya, S. Kurosawa, and N. Sarukura: Phys. Status Solidi **9** (2012) 2284. https://doi.org/10.1002/pssc.201200176
16 M. Koshimizu, N. Kawano, A. Kimura, S. Kurashima, M. Taguchi, Y. Fujimoto, and K. Asai: Sens. Mater. **33** (2021) 2137. https://doi.org/10.18494/sam.2021.3314
17 A. Horimoto, N. Kawano, D. Nakauchi, H. Kimura, M. Akatsuka, and T. Yanagida: Sens. Mater. **32** (2020) 1395. https://doi.org/10.18494/SAM.2020.2747
18 N. Kawano, A. Horimoto, H. Kimura, D. Nakauchi, M. Akatsuka, and T. Yanagida: Mater. Res. Bull. **142** (2021) 111409. https://doi.org/10.1016/j.materresbull.2021.111409
19 N. Kawano, D. Nakauchi, M. Akatsuka, H. Kimura, and T. Yanagida: J. Lumin. **241** (2021) 118467. https://doi.org/10.1016/j.jlumin.2021.118467
20 K. Shibuya, M. Koshimizu, Y. Takeoka, and K. Asai: Nucl. Instrum. Methods Phys. Res., Sect. B **194** (2002) 207. https://doi.org/10.1016/S0168-583X(02)00671-7
21 N. Kawano, M. Koshimizu, Y. Sun, N. Yahaba, Y. Fujimoto, T. Yanagida, and K. Asai: Jpn. J. Appl. Phys. **53** (2014) 02BC20. https://doi.org/10.7567/JJAP.53.02BC20
22 K. Shibuya, M. Koshimizu, H. Murakami, Y. Muroya, Y. Katsumura, and K. Asai: Jpn. J. Appl. Phys. **43** (2004) L1333. https://doi.org/10.1143/JJAP.43.L1333

23 N. Kawano, M. Koshimizu, Y. Sun, N. Yahaba, Y. Fujimoto, T. Yanagida, and K. Asai: J. Phys. Chem. C **118** (2014) 9101. https://doi.org/10.1021/jp4114305
24 N. Kawano, M. Koshimizu, A. Horiai, F. Nishikido, R. Haruki, S. Kishimoto, K. Shibuya, Y. Fujimoto, T. Yanagida, and K. Asai: Jpn. J. Appl. Phys. **55** (2016) 110309. https://doi.org/10.7567/JJAP.55.110309
25 N. Kawano, M. Koshimizu, G. Okada, Y. Fujimoto, N. Kawaguchi, T. Yanagida, and K. Asai: Sci. Rep. **7** (2017) 14754. https://doi.org/10.1038/s41598-017-15268-x
26 M. Akatsuka, N. Kawano, T. Kato, D. Nakauchi, G. Okada, N. Kawaguchi, and T. Yanagida: Nucl. Instrum. Methods Phys. Res., Sect. A **954** (2020) 161372. https://doi.org/10.1016/j.nima.2018.10.050
27 D. Nakauchi, N. Kawano, N. Kawaguchi, and T. Yanagida: Jpn. J. Appl. Phys. **59** (2020) SCCB04. https://doi.org/10.7567/1347-4065/ab515d
28 D. Onoda, M. Akatsuka, N. Kawano, D. Nakauchi, T. Kato, N. Kawaguchi, and T. Yanagida: J. Mater. Sci. Mater. Electron. **31** (2020) 20798. https://doi.org/10.1007/s10854-020-04592-0
29 D. Onoda, M. Akatsuka, N. Kawano, D. Nakauchi, T. Kato, N. Kawaguchi, and T. Yanagida: Opt. Mater. **114** (2021) 111002. https://doi.org/10.1016/j.optmat.2021.111002
30 D. Onoda, M. Akatsuka, N. Kawano, D. Nakauchi, T. Kato, N. Kawaguchi, and T. Yanagida: J. Lumin. **237** (2021) 118157. https://doi.org/10.1016/j.jlumin.2021.118157
31 D. Onoda, M. Akatsuka, N. Kawano, D. Nakauchi, T. Kato, N. Kawaguchi, and T. Yanagida: Jpn. J. Appl. Phys. (2021) (in press). https://doi.org/10.35848/1347-4065/ac1487
32 R. D. Shannon: Acta Crystallogr. Sect. A **32** (1976) 751. https://doi.org/10.1107/S0567739476001551
33 D. Onoda, M. Akatsuka, N. Kawano, D. Nakauchi, T. Kato, N. Kawaguchi, and T. Yanagida: J. Mater. Sci. Mater. Electron. **31** (2020) 20798. https://doi.org/10.1007/s10854-020-04592-0
34 T. Yanagida, K. Kamada, Y. Fujimoto, H. Yagi, and T. Yanagitani: Opt. Mater. **35** (2013) 2480. https://doi.org/10.1016/j.optmat.2013.07.002
35 T. Yanagida, Y. Fujimoto, T. Ito, K. Uchiyama, and K. Mori: Appl. Phys. Express **7** (2014) 18. https://doi.org/10.7567/APEX.7.062401
36 P. Kantuptim, M. Akatsuka, D. Nakauchi, T. Kato, N. Kawaguchi, and T. Yanagida: Sens. Mater. **32** (2020) 1357. https://doi.org/10.18494/SAM.2020.2726
37 K. Kubota, M. Koshimizu, H. Saito, and K. Asai: Bull. Chem. Soc. Jpn. **88** (2015) 1567. https://doi.org/10.1246/bcsj.20150141
38 L. Zhang, L. Wu, K. Wang, and B. Zou: Adv. Sci. **6** (2019) 1801628. https://doi.org/10.1002/advs.201801628
39 N. Kawano, D. Nakauchi, H. Kimura, M. Akatsuka, K. Takahashi, F. Kagaya, and T. Yanagida: Jpn. J. Appl. Phys. **58** (2019) 082004. https://doi.org/10.7567/1347-4065/ab2e7c
40 N. Kitazawa, M. Aono, and Y. Watanabe: Mater. Chem. Phys. **134** (2012) 875. https://doi.org/10.1016/j.matchemphys.2012.03.083
41 A. Lempicki, A. J. Wojtowicz, and E. Berman: Nucl. Inst. Methods Phys. Res., Sect. A **333** (1993) 304. https://doi.org/10.1016/0168-9002(93)91170-R